Effect of Free Surface on the Stability of Individual Retained Austenite Grains in a Duplex Stainless Steel

B.B. HE, M.X. HUANG, A.H.W. NGAN, and S. VAN DER ZWAAG

The present work explored the effect of free surface on the stability of individual austenite grains in a duplex stainless steel. It was found that martensitic transformation took place automatically in the retained austenite grain when a free surface was introduced. This is due to the fact that the martensite nucleation energy barrier can be lowered to a thermally surmountable value as the strain energy induced by martensitic transformation is largely lowered when the matrix constraints were removed.

I. INTRODUCTION

MARTENSITIC transformation (MT) plays a key role not only in shape memory alloys[1] but also in the development of high strength steels, especially transformation-induced plasticity (TRIP) steels,[2] meta-stable austenitic steels[3] and duplex steels.[4] MT in steels is a first order solid state phase transformation in which the meta-stable face-centered cubic (fcc) austenite (γ) phase transforms into body-centered cubic (bcc) or tetragonal (bct) martensite (α'). Externally applied stresses,[5] a lowering of the temperature,[6] application of a magnetic field[7] or a combination of above driving factors can affect MT. During straining of a TRIP steel, the formation of martensite provides a higher work hardening rate and delays the onset of localized plastic deformation (necking),[2] resulting in an improved combination of a high tensile strength and a high uniform elongation.[8] The occurrence of MT is closely related to the stability of the austenite grains, which depends on the chemical composition,[2] morphology,[9] grain size[10] and hardness of the surrounding grains[11] as documented in literature.

Different to the above aspects reported in literature, the present work is to explore a new factor which could also affect the stability of retained austenite, *i.e.*, the stability of an individual retained austenite grain could be affected by whether or not it is surrounded by matrix. In other words, if a retained austenite grain is free from the matrix, it may transform to martensite automatically. Focused ion beam (FIB) milling is a suitable technique to create free surfaces in individual grains. Thus, the present work employs FIB milling to create free surface around individual retained austenite grains and studies the effect of the free surface on their stability.

II. EXPERIMENTS

The material employed in this study was a duplex stainless steel with a chemical composition of Fe-0.03C-6Mn-16Cr-3Ni (wt pct). A cylindrical sample with a diameter of 10 mm and a thickness of 3 mm was cut from the bulk material. The sample surface was mechanically polished down to 1 μm and subsequently electropolished in a solution of 5 pct perchloric acid, 15 pct glacial acetic acid and 80 pct ethanol at room temperature under an applied voltage of 18 V. The austenite and ferrite grains (α) were identified by electron backscattering diffraction (EBSD, Leo 1530). For the EBSD measurement, a step size of 0.1 μm was used. HKL Channel 5 was used to process the EBSD data. After locating the individual austenite grains, the sample was transferred to the FIB (FEI Quanta 200 3D Dual Beam) chamber and the milling at selected austenite/ferrite boundaries was done with an accelerating voltage of 20 kV and a very low current of 10 pA. The surface of the austenite grain next to the slit was carefully monitored in situ during the FIB milling in order to identify local surface relief related to the occurrence of MT. Upon live observation of the local surface relieve in the austenite grain, the sample was then returned to the EBSD chamber to verify whether MT had taken place in the individual austenite grains subjected to FIB milling. By comparing the EBSD maps taken prior to the milling and the ones after the milling, the formation of new martensite was demonstrated unambiguously.

III. RESULTS

Figure 1(a) shows the EBSD phase map of the duplex stainless steel prior to FIB milling. The phase colored in red is ferrite and that colored in yellow is austenite. Each austenite grain was typically surrounded by several smaller bcc ferrite grains and the total volume fraction

B.B. HE, Ph.D. Candidate, M.X. HUANG, Assistant Professor, and A.H.W. NGAN, Professor, are with the Department of Mechanical Engineering, The University of Hong Kong, Pokfulam Road, Hong Kong, P. R. China. Contact e-mail: mxhuang@hku.hk S. VAN DER ZWAAG, Professor, is with the Faculty of Aerospace Engineering, Delft University of Technology, Kluijverweg 1, 2629 HS Delft, The Netherlands.

of austenite was estimated to be 45 pct. The average austenite grain size is 15 μm. Such a large grain size is desirable for the present study as MT in large austenite grains may lead to noticeable surface relief which can be captured live by in situ scanning electron microscope (SEM) observation during FIB milling. As labeled in Figure 1(a), two zones each containing one individual austenite grain were selected for the FIB cutting experiment. Figure 1(b) is the corresponding EBSD orientation map, showing the initial orientation of the selected individual austenite grains. The single austenite grain in Zone 1 contained two annealing twins with the same orientation but different sizes, while the individual austenite grain in Zone 2 was intersected by a small ferrite grain.

Figure 2(a) is a SEM image of Zone 1 captured during the FIB cutting experiment. It shows a straight slit with a width and depth of about 1 μm. During the FIB milling, the first lath shaped surface protrusion (within the yellow circle) was formed next to the slit on the flat surface of the austenite grain. As the slit was further deepened by FIB milling, a second surface protrusion (Figure 2(b)) was formed parallel to the first one. These surface protrusions in Figures 2(a) and (b) correspond to the shear shape deformation of MT. Figure 2(c) shows the EBSD phase map of the austenite

grain after the FIB cutting experiment. Comparison of this phase map to the original one in Figure 1(a) confirms that the crystal structure has indeed changed from fcc to bcc at the site of the surface protrusions. Figure 2(d) shows that the original annealing twins (Figure 1(b)) disappeared after the FIB milling, indicating that the annealing twin boundary may not be able to inhibit the growth of martensite. On the contrary, it may facilitate the growth of martensite as the direction of surface relieves (Figure 2(b)) was perfectly coincident with the direction of annealing twin boundary. A minimal orientation spread (~3 deg) within the martensite was observed. Figure 2(e) is the corresponding image quality (IQ) map. It shows that the IQ value in the untransformed austenite phase is higher than that in the martensite phase. Moreover, the IQ value also differs among the transformed regions, depending on the distance to the slit, e.g., the IQ value of the region within the red circle is obviously higher than that within the green ellipse. The lath boundary of the martensite is not clear in the IQ map and this may be due to the limited EBSD resolution and the fine structure of martensite in the duplex stainless steel. Each single surface relief in Zone 1 may be classified as a packet of martensite containing groups of lath martensite with a common habit plane.

In order to verify the repeatability of observed phenomenon, another FIB cutting experiment was performed in the austenite grain in Zone 2. Figure 3(a) is the SEM image of Zone 2 before the FIB cutting experiment, providing the original reference state. The region within the black ellipse contains the austenite grain of interest and it had a relatively featureless surface. Figure 3(b) is a SEM image of the same area after the FIB cutting experiment. The first slit was made in the middle of the austenite grain, while the second one was made close to a grain boundary of the austenite to separate it from the surrounding ferrite phase. Based on these two SEM images, it was difficult to determine whether MT had taken place as no obvious surface relief can be observed. Further EBSD evidence on MT was required. Figure 3(c) shows the EBSD phase map of the same area after the FIB cutting. Compared to the EBSD phase map before FIB cutting (Figure 1(a)), it can be found that the crystal structure has changed from fcc to bcc at the upper part of the austenite grain, confirming that MT had taken place there. However, the lower part of the austenite grain was left untransformed. The grain boundary of upper part was partly removed by the FIB, while the grain boundary in the lower part was kept intact due to the small pre-existing ferrite (Zone 2 in Figure 1(b)). Figure 3(d) is the corresponding EBSD orientation map. It reveals the presence of two twin related martensite variants (60 deg/$\langle 111 \rangle \alpha'$ or $\Sigma 3$). Figure 3(e) is the EBSD IQ map. It shows that the packet of martensite in the upper austenite grain consists of several blocks with very clear boundaries observed. The IQ value of the transformed region decreases with the increasing distance from the slit, e.g., the IQ value of transformed martensite in yellow circle is higher than that in red circle. Such a gradient in IQ is consistent with the observations in Zone 1.
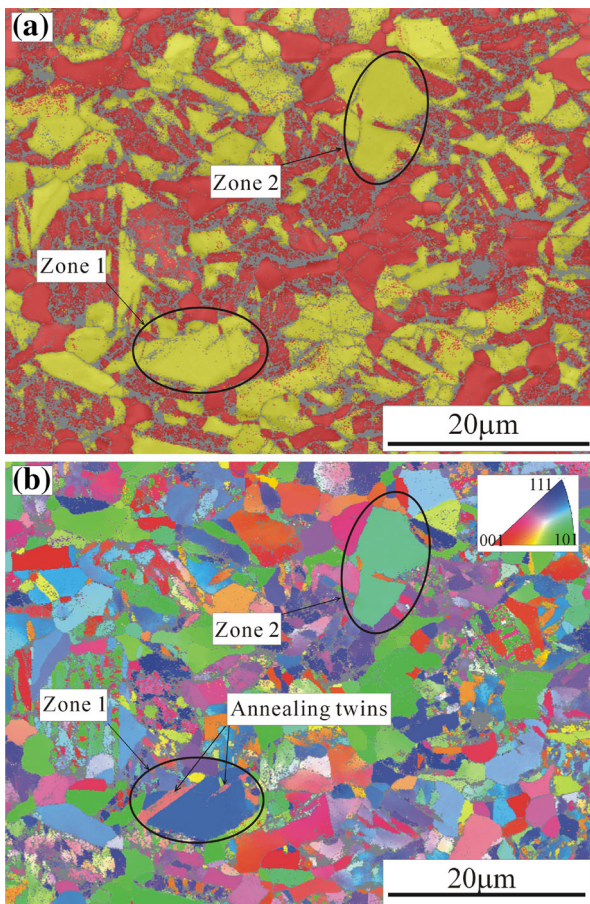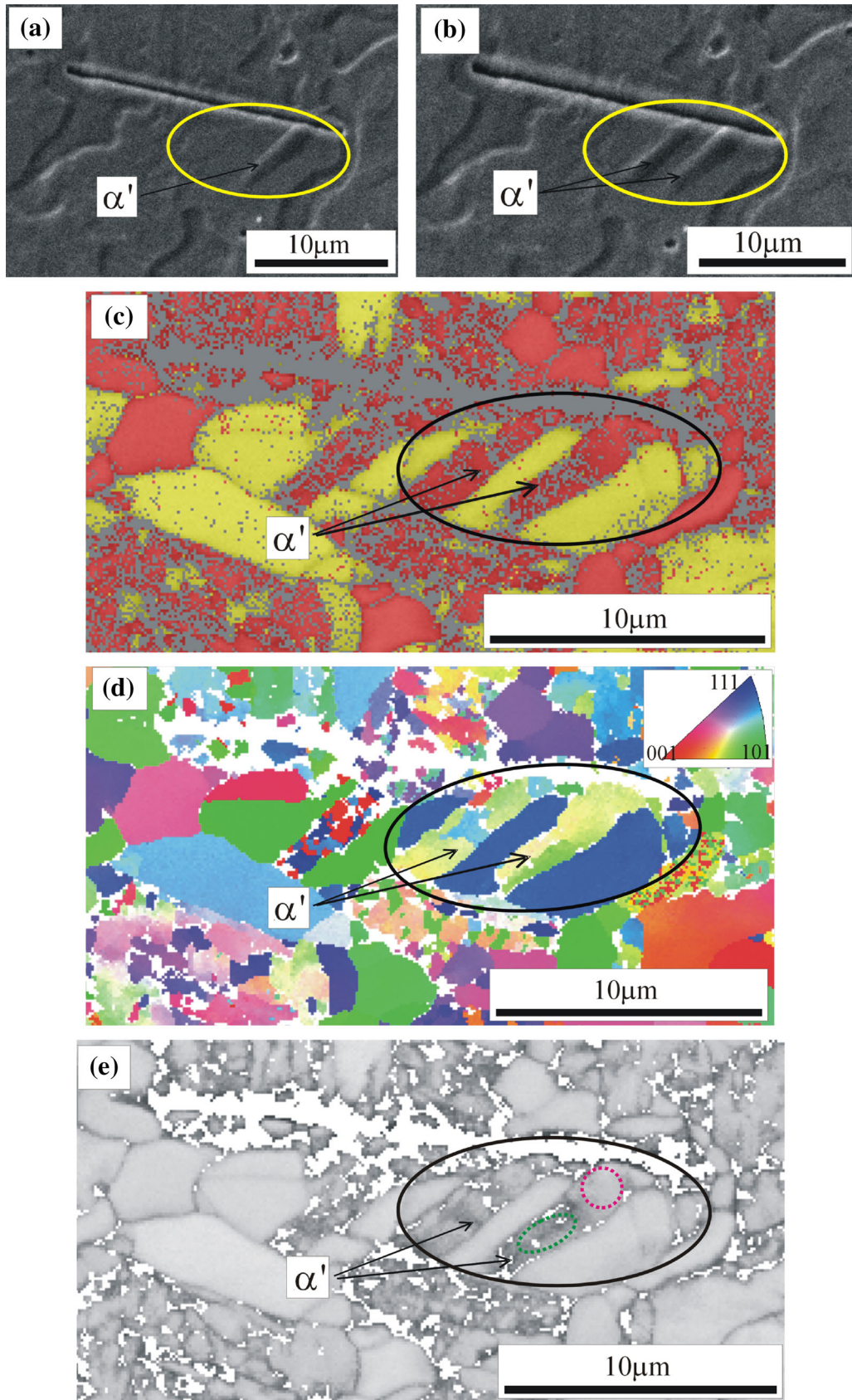

Fig. 1—(a) EBSD phase map of a duplex stainless steel (red: ferrite; yellow: austenite); (b) EBSD orientation map. The color images can be obtained in the online version of this article.

Fig. 2—(*a*) SEM images of Zone 1 for initial cut and (*b*) further cut (α′: martensite); (*c*) EBSD phase map after FIB cutting; (*d*) EBSD orientation map after FIB cutting; (*e*) EBSD image quality map after FIB cutting, broken circles are marked for comparison. The color images can be obtained in the online version of this article.
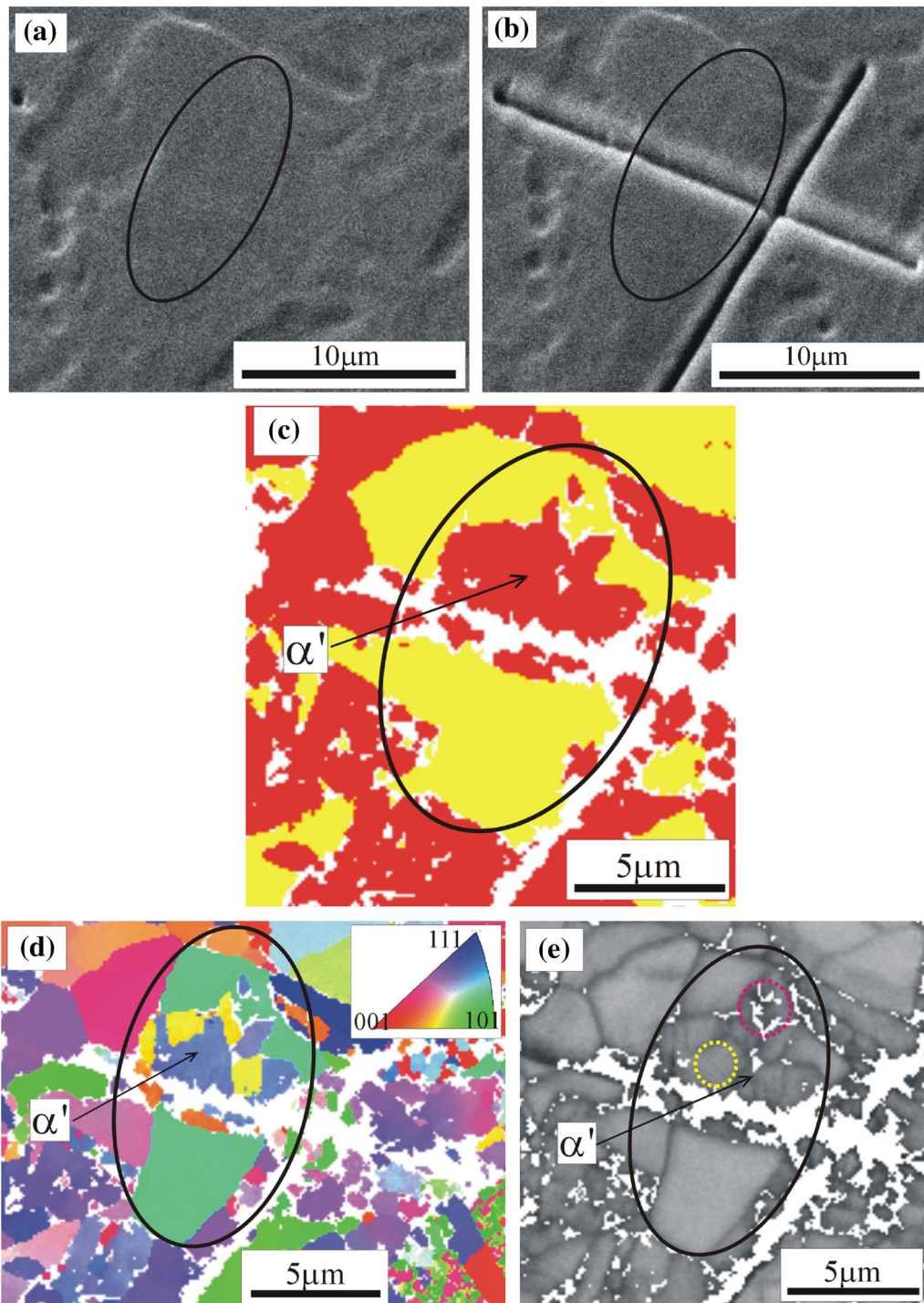
Fig. 3—(a) SEM images of Zone 2 before FIB cutting and (b) after FIB cutting; (c) EBSD phase map (α′: martensite); (d) EBSD orientation map; (e) EBSD image quality map, broken circles are marked for comparison. The color images can be obtained in the online version of this article.

IV. DISCUSSION

The nucleation of martensite has been discussed extensively in literatures.[12,13] It has been suggested that the grain boundary and free surface are the potent nucleation sites for martensite.[13] The investigated austenite grains were surrounded by the ferrite grains (Figure 1(a)), so it may be reasonable to assume that the

martensite nucleates at the γ/α interface during continuous cooling experiment. Then, this nucleation of martensite shall create the α/α' interface and γ/α' interface. Assume that a martensite nucleus is in a form of an oblate spheroid with a radius of a and a semi-thickness of c, as schematically illustrated in Figure 4. The Gibbs free energy (ΔG) for a nucleation of

martensite at the γ/α interface takes the following form,[12]

$$\Delta G = \frac{4}{3}\pi a^2 c \Delta g + f_{\alpha/\alpha'}\chi_{\alpha/\alpha'} + f_{\gamma/\alpha'}\chi_{\gamma/\alpha'} + \frac{4}{3}\pi a^2 c\left(\frac{c}{a}A_s + A_\delta\right)$$

[1]

where Δg is the chemical free energy change per unit volume, which itself depends on the alloying element concentrations and the temperature. f is the interfacial area. χ is the interfacial energy per unit area. The subscript represents the kind of interface created during nucleation of martensite. The total interfacial area for the martensite nucleus is $2\pi a^2$ in a first approximation. $A_s = \pi(2 - v)\mu s^2/8/(1 - v)$ is the shear strain energy[14] and $A_\delta = 2\mu(\delta)^2(1 + v)/(1 - v)$ is the dilatation strain energy.[15] δ and s are the dilatation strain and shear strain, respectively. v is the Poisson's ratio and μ is the shear modulus.

The value of $f_{\gamma/\alpha'}$ and $f_{\alpha/\alpha'}$ depends on the orientation of martensite nucleus at the γ/α interface. The maximum value of $f_{\alpha/\alpha'}$ should be πa^2 which is a scenario that the martensite nucleus orients along the γ/α interface and is considered in the following discussion. The Nucleation of martensite becomes possible when the nucleation barrier (ΔG^*) is thermally surmountable.[16] The nucleation barrier can be obtained by searching for the saddle point where $\frac{\partial \Delta G}{\partial a} = \frac{\partial \Delta G}{\partial c} = 0$ and is therefore expressed as follows:

$$\Delta G^* = \frac{4\pi(A_s)^2\left(\chi_{\gamma/\alpha'} + \chi_{\alpha/\alpha'}\right)^3}{3(\Delta g + A_\delta)^4}$$

[2]

The present experimental results showed that once the austenite grain boundary and the mechanical contact to the surrounding ferrite grains was removed by FIB milling, the austenite grain became unstable and MT took place. As the temperature at the FIB chamber was kept constant, Δg remains constant during the FIB cutting experiment. So it can be concluded here that the martensite formation in the present experiment is not governed by the chemical driving force. This is completely different from the continuous cooling experiment where the enhanced value of Δg results in a smaller ΔG^* and thus drives the martensite formation. Figure 2(c) through (e) and Figure 3(c) through (e) show that the
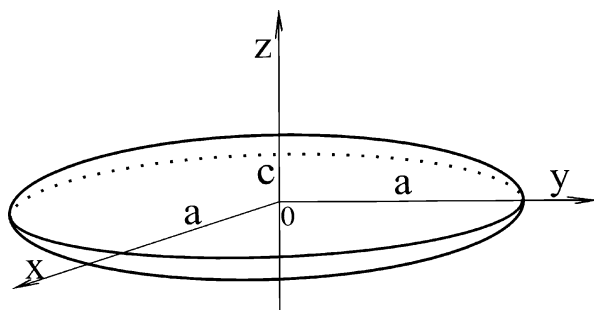
new lath martensite touched the slit which was at the γ/α interface. This suggests that martensite which should nucleate at the γ/α interface can also nucleate on the γ free surface. Considering a scenario that the martensite nucleus orients along the new free surface, then the area for free surface/α' interface is πa^2. Since the interfacial energy value of surface/α' is zero and the interfacial energy value of γ/α' is constant during the experiments, the formation of new free surface can slightly decrease ΔG^*. But it is still much larger than the thermal fluctuation. This is confirmed from literature[17] that the nucleation barrier is thermally insurmountable even when the interfacial energy was decreased by a factor of ten. So the change of the interfacial energy or interfacial area due to new free surface is insufficient to induce the nucleation of martensite. According to Eq. [2], the nucleation of martensite in the present experiment is possible when the strain energy (A_s and A_δ) was decreased to a magnitude that the resultant ΔG^* is thermally surmountable. It is noted here that a decrease of A_δ can lead to a smaller ΔG^*. This is due to the fact that Δg is a negative value and the absolute value of Δg is larger than that of A_δ. The energy barrier can be lowered by creating an additional free surface (Figures 2(b), 3(b)) as this new surface removes the constraints imposed by the surrounding austenitic matrix. The higher IQ value indicates a lower dislocation density.[18] So the martensite blocks which transformed close to the slit has a lower dislocation density than that transformed far away from the slit, confirming the relaxation effect of free surface on the martensite formation. The surface protrusion normal to the sample
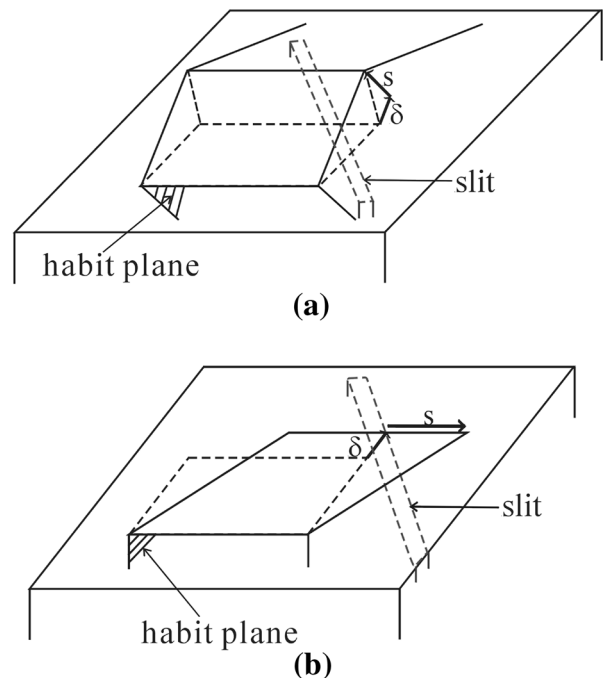
Fig. 5—schematic illustration of a martensite variant shearing (a) with at least a component (either dilatation δ or shear s or both) not on the specimen surface and a habit plane inclined to specimen surface, and (b) with both dilatation δ and shear s on specimen surface and a habit plane normal to specimen surface.

Fig. 4—Schematic illustration of a martensite nucleus (a: radius, c: semi-thickness).

Table I. Misorientation Angles and Axis Between α′ and γ for Different Orientation Models[26]

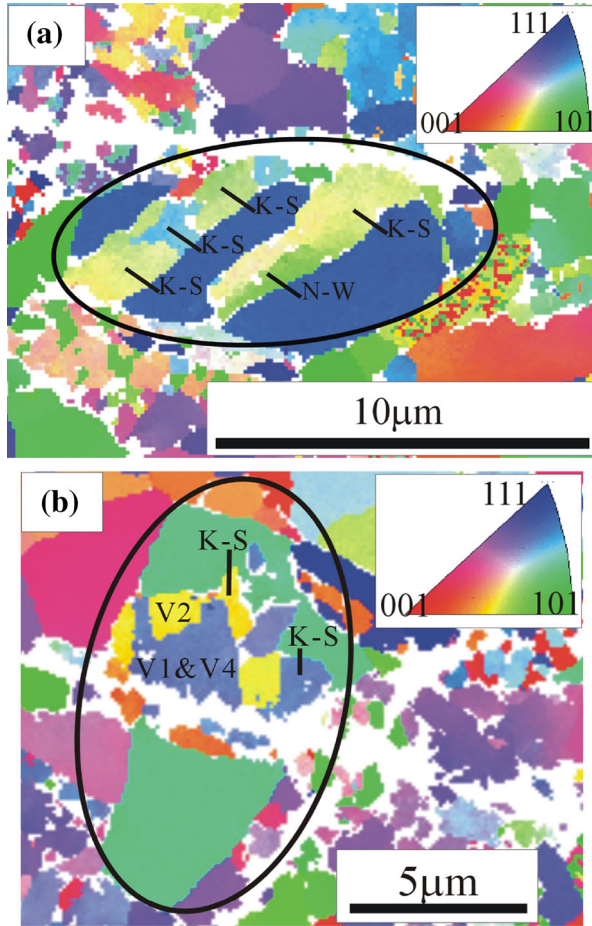| Orientation Model	Misorientation Angle (deg)	Axis
K–S	42.85	⟨17.8 17.8 96.8⟩
G–T	44.26	⟨12.2 18.4 97.5⟩
N–W	45.99	⟨8.3 20.1 97.6⟩
Bain	45.00	⟨0 0 1⟩

Fig. 6—The OR between martensite variants and the surrounding austenitic matrix in (a) Zone 1 and (b) Zone 2. The deviation angles between measured and theoretical values are generally about 1.2 deg for K–S OR and 0.8 deg for N–W OR. The color images can be obtained in the online version of this article.

surface (Figure 2(b)) indicates that at least one of the dilatation δ or shear s of martensite variant is inclined to the sample surface,[19] as schematically illustrated in Figure 5(a). Compared to the surface protrusion in Zone 1 (Figure 2(b)), the absence of obvious surface relief in Zone 2 (Figure 3(b)) indicates that martensite shears with both the dilatation δ or shear s components roughly on the specimen surface, as schematically illustrated in Figure 5(b). As Figure 5 shows, the surrounding austenitic matrix and product martensite has to deform to accommodate the shape change of martensite, resulting in strain energy stored. The newly created slit leads to a reduction of the strain energy by introducing new traction free surface.

Finally, it is appropriate to analyze the crystallography aspect of martensite formation in the present experiment. The orientation relationship (OR) between martensite and austenite can be described by several available orientation models, such as Kurdjumov–Sachs (K–S) relation,[20] Nishiyama–Wassermann (N–W) relation,[21] Greninger–Troiano (G–T) relation,[22] and Bain relation.[23] According to these orientation models, the coordinate system of a bcc crystal can rotate about a certain axis for a certain angle to coincide with the coordinate system of an fcc crystal. The misorientation angle and axis for these models are listed in Table I. By comparing the experimentally obtained misorientation angle and axis with the theoretical ones, the OR between martensite and austenite can be determined. The results of OR in Zone 1 and Zone 2 are shown in Figures 6(a) and (b), respectively. The deviations between experimentally obtained angles and theoretical ones are ~1.2 deg and ~0.8 deg for K–S and N–W OR, respectively. It is noted that most of the martensite variants obey the K–S relation as shown in Figure 6. The change of OR from K–S to N–W in the first surface relief (Figure 6(a)) may be due to the accommodation of transformation misfit within austenitic matrix.[24]

As K–S is the main OR found in the present experiment, its related variants are discussed in the following. The K–S orientation model ({111}γ ∥ {011}α′, ⟨-101⟩γ ∥ ⟨-111⟩α′) shows that 24 equivalent crystallographic martensite variants can be found within a single austenite grain. These martensite variants can be grouped into four packets of which each six variants in a packet share the same habit plane. Table II presents the six martensite variants in Packet 1 denoted from V1 to V6. More detailed descriptions on martensite variants

Table II. The Definition of K–S Variants in the Packet 1[25]

Variant	Parallel Planes	Parallel Directions	Misorientation Angle/Axis from V1
V1	(111)γ ∥ (011)α′	[-101]γ ∥ [-1-11]α′	—
V2	(111)γ ∥ (011)α′	[-101]γ ∥ [-11-1]α′	60.00/[11-1]α′
V3	(111)γ ∥ (011)α′	[01-1]γ ∥ [-1-11]α′	60.00/[011]α′
V4	(111)γ ∥ (011)α′	[01-1]γ ∥ [-1-11]α′	10.53/[0-1-1]α′
V5	(111)γ ∥ (011)α′	[1-10]γ ∥ [-1-11]α′	60.00/[0-1-1]α′
V6	(111)γ ∥ (011)α′	[1-10]γ ∥ [-11-1]α′	49.47/[011]α′

can be found in.[25] Kitahara *et al.*[25] show that the austenite grain can be transformed into a martensite variant through an orientation transformation matrix which is unique for a single variant. The orientation transformation matrix is independent of prior austenite orientation. In principle, the martensite variants can be determined by comparing the experimentally obtained orientations with the theoretical ones which were reported in.[25] However, this method is not adequate to determine the martensite variants in Zone 1 as these variants transformed both from annealing twin and austenitic matrix. Therefore, only variants in Zone 2 are analyzed as illustrated in Figure 6(b). The twin related martensite variants (V1 and V2) dominate the whole packet. A sub-block (V4) which has a small misorientation with V1 along the $\langle 0\text{-}1\text{-}1 \rangle \alpha'$ axis is also determined but its volume fraction is much smaller.

V. CONCLUSIONS

Different to other well-known factors affecting the stability of retained austenite grains, the present work explored a new factor which can also affect the stability of retained austenite grain, *i.e.*, the effect of free surface on the stability of individual retained austenite grains. It was found that martensitic transformation took place automatically in the retained austenite grain when the free surface was introduced in individual retained austenite grains. The strain energy stored during the nucleation of martensite can be lowered by introducing a new free surface as this free surface can relax the constraints imposed by the austenitic matrix. The lowering of strain energy can reduce the martensite nucleation energy barrier to below the thermal fluctuation so that spontaneous martensite formation took place.

REFERENCES

1. L. Delaey, R.V. Krishnan, H. Tas, and H. Warlimont: *J. Mater. Sci.*, 1974, vol. 9, pp. 1521–35.
2. P.J. Jacques: *Curr. Opin. Solid State Mater. Sci.*, 2004, vol. 8, pp. 259–65.
3. H.N. Han, C.G. Lee, C.-S. Oh, T.-H. Lee, and S.-J. Kim: *Acta Mater.*, 2004, vol. 52, pp. 5203–14.
4. C. Herrera, D. Ponge, and D. Raabe: *Acta Mater.*, 2011, vol. 59, pp. 4653–64.
5. J.R. Patel and M. Cohen: *Acta Metall.*, 1953, vol. 1, pp. 531–38.
6. E. Jimenez-Melero, N.H. van Dijk, L. Zhao, J. Sietsma, S.E. Offerman, J.P. Wright, and S. van der Zwaag: *Acta Mater.*, 2007, vol. 55, pp. 6713–23.
7. D. San Martin, N.H. van der Dijk, E. Brück, and S. van der Zwaag: *Mater. Sci. Eng. A*, 2008, vols. 481–482, pp. 757–61.
8. O. Bouaziz, H. Zurob, and M. Huang: *Steel Res. Int.*, 2013, vol. 84, pp. 937–47.
9. X.C. Xiong, B. Chen, M.X. Huang, J.F. Wang, and L. Wang: *Scripta Mater.*, 2013, vol. 68, pp. 321–24.
10. S. Lee, S.J. Lee, and B.C. De Cooman: *Scripta Mater.*, 2011, vol. 65, pp. 225–28.
11. T.D. Tjahjanto, A.S.J. Suiker, S. Turteltaub, P.E.J. del Rivera Diaz Castillo, and S. van der Zwaag: *Comput. Mater. Sci.*, 2007, vol. 41, pp. 107–116.
12. L. Kaufman and M. Cohen: *Prog. Metal Phys.*, 1958, vol. 7, pp. 165–246.
13. P.C. Clapp: *Phys. Status Solidi (B)*, 1973, vol. 57, pp. 561–69.
14. J.W. Christian: *Acta Metall.*, 1958, vol. 6, pp. 377–79.
15. T. Mura: *Micromechanics of Defects in Solids*, 2nd ed., Martinus Nijhoff, Dordrecht, 1987, pp. 112–18.
16. T.Y. Hsu: *Mater. Sci. Eng. A*, 2006, vols. 438–440, pp. 64–68.
17. H. Knapp and U. Dehlinger: *Acta Metall.*, 1956, vol. 4, pp. 289–97.
18. M. Calcagnotto, D. Ponge, E. Demir, and D. Raabe: *Mater. Sci. Eng. A*, 2010, vol. 527, pp. 2738–46.
19. M.X. Zhang and P.M. Kelly: *Prog. Mater. Sci.*, 2009, vol. 54, pp. 1101–70.
20. G.V. Kurdjumov and G. Sachs: *Z. Phys.*, 1930, vol. 64, pp. 325–43.
21. G. Wassermann and K. Mitt: *Inst. Eisenforsch*, 1935, vol. 17, p. 149.
22. A.B. Greninger and A.R. Troiano: *Trans. AIME*, 1940, vol. 140, p. 307.
23. E.C. Bain and N.Y. Dunkirk: *Trans. AIME*, 1924, vol. 70, pp. 25–35.
24. H. Sato and S. Zaefferer: *Acta Mater.*, 2009, vol. 57, pp. 1931–37.
25. H. Kitahara, R. Ueji, N. Tsuji, and Y. Minamino: *Acta Mater.*, 2006, vol. 54, pp. 1279–88.
26. S. Zaefferer, J. Ohlert, and W. Bleck: *Acta Mater.*, 2004, vol. 52, pp. 2765–78.